THIS PAPER MUST BE CITED AS:

Thin Solid Films 495 (2006) 29 – 35

MANUSCRIPT COVER PAGE FORM

E-MRS Symposium : **Symposium E : Synthesis, Characterization and Applications of Mesostructured Thin Layers**

Paper Number : **E/PI.01**

Title of Paper : **Electroforming processes for platinum nanoisland thin films**

Corresponding Author : **Cristina Bertoni**

Full Mailing Address :

Nanotechnology Group
Cranfield University
SIMS B70
Cranfield Bedfordshire MK43 0AL
ENGLAND

Telephone : **+44 (0) 1234 750111 ext. 2422**
Fax : **+44 (0) 1234 751346**
E-mail : **c.bertoni@cranfield.ac.uk**

Electroforming processes for platinum nanoisland thin films

C. Bertoni, D. E. Gallardo, S. Dunn

Nanotechnology Group, School of Industrial and Manufacturing Science

Cranfield University, Cranfield, Bedfordshire MK43 0AL England

Tel +44 (0) 1234 750111 ext 2422 Fax +44 (0) 1234 751346

Email contact: c.bertoni@cranfield.ac.uk

Abstract

An investigation of the electroforming processes for platinum discontinuous thin films is detailed. Current-voltage characteristics, for metal nanoislands deposited by sputtering, were obtained in vacuum and air and typically showed voltage-controlled negative resistance (VCNR) behaviour. The current maximum shifted with the electrode separation. Electroforming under high current density regimes was non-regenerative as samples showed irreversible resistance changes. SEM examination of the film revealed a change in the metal microstructure. Such modifications arise as a result of the current flowing through the film inducing electro and thermal migration. Current-induced effects were studied by modelling the metal nanoisland (MN) layer as an array of cubic cells. Plots of current distribution showed that hot-spots develop along conductive paths. Electromigration combined with resistive heating can lead to progressive destruction of current channels at these hot-spots. Hence, current profiles and SEM micrographs were interpreted as evidence of a 'macroscopic' electrical breakdown of sample conduction due to microstructural modifications of the thin

film. The reduction of ohmic component and consequent resistive heating along the current channels prevented the metal migration and stable current profiles were obtained.

Keywords: electromigration, discontinuous metal thin films

1. Introduction

Research activity on nanophase materials has seen a tremendous growth in the last decade. Investigation of nanometer-sized materials has attracted considerable attention because of their unique chemical/physical properties when compared to solid-state bulk materials as well as their potential in nanoscale devices.

The development of chemical and physical routes to make self-organised MN arrays has seen a renewed interest due to their relevance in several fields of research. A major technology objective is the ability to control size/distribution of nano-particles over large areas. As reported in [1], size/shape of metal particles influence the chemisorption and catalytic activity in metal-on-oxide systems. They are also critical in determining the optical properties of metal-dielectric nanocomposites thin films [2].

There is considerable interest in using ordered MN layers as a method for fabricating intrinsic nanoscale devices. Currently the design of nanostructures is unachievable through standard UV-lithography and is expensive and time-consuming using e-beam techniques. Self-assembled nanoisland arrays could serve as templates for the growth of ordered patterns of quantum structures and, hence, the design of novel electronic and optical devices. For instance,

MN can be used as catalyst sites for carbon nanotubes [3] and ZnO nanorods growth [4]. Here, the size of the catalyst metal particles determines the growth properties of the quantum structures.

In optoelectronics, conduction and optical properties of MN layers have been used to enhance carrier transport and injection in multilayer devices. As shown in [5], optically transparent MN thin layers can enhance carrier injection and therefore, device efficiency in OLED. Again, the metal particles size and separation is critical in determining optical transmission of the layer and conduction properties of the overall device.

High work function metals in the form of ultra thin discontinuous electrodes have been investigated as injection layers for a novel low-voltage thin film electroluminescent device. As the device operation requires high in-plane current densities at low applied voltages (≤10V), it was necessary to find optimal MN size and distribution to avoid metal migration under the application of an external electric field. Electro and thermo migration processes are known in the semiconductor industry causing damage to metal interconnects and eventual device failure [6, 7]. Ichinokawa and co-workers [8] showed that such phenomena also affect ultra thin metal films. Various metal films were vacuum evaporated onto a p-type Si (001) wafer. Heating to 500˚C caused the nucleation of metal islands. Electromigration of micron size islands proceeded on Si substrates in the presence of an electric field or electric current. The large islands migrate while coalescing with the small islands and increasing diameters. The migration velocity increases with the substrate temperature and island radius.

Qualitative description of electroforming can be found in [9], a review devoted to electron and light emission from metal nanodispersed films. A typical device structure consists of two metal electrodes ~100nm thick with a gap of *ca* 10μm deposited onto a dielectric substrate. The metal layer is usually vacuum-evaporated and electroformed by applying a voltage of 20-30V for 0.5-2min. Electron and photon emission centres which are ≤1μm in size are believed to arise as a result of electro/thermomigration processes occurring during the electroforming. Conduction currents in electroformed films are a few mA and are non-linear. The effect of overlayers on light emission from metal islands was studied by coating pre-formed islands with organic molecules layers (e.g., stearone). I-V curves revealed an increase in the overall sample conduction, related to organic conducting bridges spanning the gaps between islands, and the occurrence of VCNR behaviour.

VCNR behaviour was also observed in metal-insulator-metal (MIM) structures [10]. The MIM device family consists of multilayer structures where the insulating material (5nm to 1μm thick) is sandwiched between the metal electrodes and open planar devices where a thin or semi-continuous metal film is deposited between two planar metal electrodes. In the latter case, the metal film thickness is initially about 10nm, while the actual MIM element is then obtained by thermal annealing with consequent rupturing of the metal film and creation of a microslit (~1μm broad). Residual metal coagulates into islands located between the electrode edges. Typical I-V curves reported for planar devices present non-ohmic profiles at low voltages followed by a current maximum (~100mA) and a negative differential resistance region. In particular, the first up-ramp is characterised by a steep positive slope until an inflexion point where an overall decrease in sample conductance is detected.

The aim of the present work is to produce and electrically characterise Pt nanoisland thin films which could be used as large area (5–30mm^2), highly efficient carriers' injection layers for a planar device structure. Pt was selected because of its high work function and resistance to oxidation. In this paper, current induced effects occurring during electroforming of ultra thin MN layers are studied. Initial experiments were carried on very thin Pt layers (~2nm) which showed, as observed in the SEM, an island structure and good conductive properties (<ρ>=60μΩcm). The procedures to grow nanoscale Pt islands by RF sputtering techniques are reported.

2. Experimental

2.1 Preparation of MN thin films

Deposition experiments to obtain MN on dielectric substrates were carried in a high vacuum sputtering system (Nordiko2500) at a base pressure of 8-10×10^{-7}mbar using DC magnetron sputtering. Substrates were initially cleaned by organic solvents (acetone and isopropanol) rinse at room temperature (RT) in an ultrasonic bath for 15min.

Ultra high precision SEM micrographs of both as-deposited and electroformed films were taken using a field emission gun (SFEG) XL30 Philips apparatus.

2.2 Electrical characterisation

Rectangular Cr/Au electrodes 10mm large and spaced from 0.5 to 3.5mm were thermally evaporated. Once the discontinuous metal layer was deposited, DC voltage sweeps of ~0.1V/s

were applied to the MNs film using a DC power supply (3A-60V) while the current was measured using an HP34410A multimeter. I-V experiments were carried at RT under high vacuum (HV) conditions (at ~10^{-6}mbar) and in air.

Linear resistance (*LR*) was introduced as a reference parameter to compare results obtained across different areas. It is defined as the ratio between the initial resistance measured across an electrodes' pair in vacuum and the distance of separation.

3. Results and discussion

3.1 MN thin film deposition and characterisation

Experiments were conducted to determine the optimal sputtering conditions for the MN on a series of substrates taking into account the interaction of surface free energy on nucleation [11]. Soda lime glass slides and SiO_2(400nm)/Si wafers were used for these experiments – glass being selected for the following I-V study. The sputtering power was decreased and a discontinuous film was obtained at 30W and 20W, as revealed by SEM examination. Figures 1a and b depict the film morphology for Pt sputtered on glass and SiO_2/Si at 30W for 10s. As can be seen, the metal nanostructure does not change significantly on different substrates. This was attributed to typical Pt behaviour of forming a dense population of nuclei coalescing to form large aggregates at low average film thickness [11]. Control of deposition allows growth to be stopped during coalescence, films obtained on different substrates present similar patterns.

Contrast and resolution achieved in imaging MNs on SiO_2/Si allowed measuring islands' size and separation. The average gap measured between nanoislands was less than 3nm. Using deposition rate measurements the layer thickness was estimated at less than 2nm.

3.2 I-V characteristics, morphological analysis and percolation modelling of low LR samples (~10^4Ω/m) characterised by >60% metal surface coverage

The metal surface coverage for MN thin films obtained at 30W for 10s on glass was calculated through image processing of the SEM micrographs. The images were digitalised using Adobe Photoshop 6.0 and a threshold method [12] was applied. The percentage of non conductive pixels *Pb* vs. the digitalisation level *I* was derived. The derivative d*Pb*/d*I* shows a peak corresponding to the most significant change in the pattern with the digitalisation level when the background pixels are separated from 'conductive' pixels.

The *Pb* calculated from large area images (figure 1b) was around 35%. Therefore, the estimated surface coverage for the metal layers is about 65%.

The following discussion is focussed on short distance electrode pairs, i.e. 0.5 and 1mm. Large electrode separation areas exhibited low current densities both in vacuum and in air. Hence, only some results concerning large electrode separation are reported for comparison (table 1).

Figure 2 shows I-V curves obtained by applying slow velocity (~0.1V/s) DC voltage sweeps up to 10V across different areas over the same sample (S1, $<LR>=3\times10^4\Omega$/m) under HV and

air. In both cases, curves are ohmic at low electric fields and show a slow and ‘noisy’ decrease in conductance until a current maximum and negative resistance region are reached. Furthermore, it can be observed that the critical voltage V_C at which the current starts to breakdown shifts with electrodes separation (table 1).

SEM analysis (figures 3a and b) revealed that migration processes had led to the formation of a filaments network. The evolution of electro and thermo- migration processes tends to form and destroy the filaments under vacuum while it leaves them intact in air.

These morphological changes in metal nanostructure were interpreted as evidence of production of conductive filaments under the influence of intense electric field as proposed to account for VCNR behaviour in sandwich-type and planar MIM structures [10, 13]. In this model, maximum current occurs when the filaments matrix consists of a large number of conducting paths, while the final decrease in current corresponds to filaments rupture due to high local Joule heating. The decrease in conduction found for this type of films (S1s) during the up-ramps suggests a high rate of filaments rupture at all V’s.

Samples of similar initial resistance R_0 show similar I-V slopes (figure 2) however conduction breakdown occurs earlier under vacuum than in air. This is explained as a consequence of local reactions (pyrolisis) involving organic molecules adsorbed on the surface and subsequent production of carbon bridging the islands [14], so that current is shared by many conductive paths reducing the amount of heat generated locally.

Furthermore, samples characterised in air show a degree of ‘filaments regeneration’, while filaments rupture predominates under vacuum and leads to irreversible changes in sample conduction (figure 4). This can be ascribed to the adsorption of organic molecules which act as constructive building blocks of new conductive bridges between the islands.

SEM/EDX analyses were conducted on samples electrically characterised in vacuum and air. Spectra were acquired at 5keV and all chemical elements related to the typical composition of soda lime glasses were detected. Different spectra were compared by equating the Ca content in correspondence to the L-line at 0.305keV. The comparison qualitatively indicates a larger percentage of carbon (K-line at 0.29keV) in the composition of samples characterised in air (figure 5).

Currents through percolated layers in vacuum were studied by simulating the MN layer as an array of 3D cells. A code was created in Visual C++ to generate a random configuration of metallic and empty cells from a specified set of parameters, such as cell dimensions and occupational probability. A series of simulations were run for occupational probabilities >60% (figure 6a) by assuming ohmic conduction through percolation paths. For a given voltage, the program calculates the potential and current distributions for the generated pattern. Figure 6b shows that current is concentrated along low resistance percolation paths within the pattern. These filaments present ‘hot-spots’ where the current reaches maximum values. Current densities estimated at these points were in the range of $10^7 A/cm^2$. These values support the hypothesis that Joule heating developed locally could cause the rupture of the filament.

The shift of critical voltage with electrodes separation further confirms this hypothesis: as the length of spanning clusters increases with distance between the electrodes, the current density will on average decrease with electrode distance. As a consequence, the process of overheating and filaments rupture will be delayed to higher applied voltages.

3.3 I-V characteristics and morphological analysis of high LR (~10^5-10^6Ω/m) samples characterised by <60% surface coverage

To avoid major morphological changes and increase reproducibility, it was necessary to reduce the probability of formation of spanning clusters between the electrodes. It is possible to stop the deposition process at a MN distribution characterised by a lower number of spanning clusters by monitoring the thin film resistance during deposition.

New samples were obtained by sputtering under normal conditions and monitoring the resistance across areas of interest (table 1, samples S2 and S3). Surface coverage for these samples was determined using the digitalisation level method and was around 55%.

Figures 7a and b show MNs' distribution on glass corresponding to samples S2 and S3 characterised by a *LR* of 10^5 and 10^6Ω/m respectively. In particular, MNs associated with figure 7b are separated by larger gaps (~5nm). Both images present 'bright' spots due to charging effects.

Results of I-V experiments carried in vacuum at RT are reported in figure 9. After an initial ohmic behaviour the current increases non-linearly with the applied voltage. This is different

from what was found in low *LR* samples where the initial up-ramp shows a slow and progressive decrease in the sample conductance (figure 2 or 5). The current flowing trough sample S2 is still important and the electrical conduction failed at about 10V. Conversely, the current profile obtained for sample S3 over the same voltage range is characterized by lower current densities and did not exhibit electrical breakdown.

Subsequent SEM examination (figure 8a and b) revealed that the forming process has slightly affected the metal nanostructure compared to the initial state (figure 7a and b). However the film morphology still consists of isolated nanoislands. In both cases it is still possible to determine the shape and separation of electroformed MNs.

From these results, it is possible to infer that the morphology of Pt nanoisland thin films is preserved in high surface coverage samples (~55%) where the power supplied to the system can be dissipated without inducing major electromigration processes.

4. Conclusions

A process for depositing Pt MN thin layers by sputtering techniques was evaluated and used to make films that are consistent and can be investigated in terms of I-V. A range of experiments were conducted in HV and air on conductive Pt nanoisland thin films.

For over 60% surface coverage samples, typical I-V curves exhibited a VCNR-like behaviour with a current maximum followed by a negative resistance region. The current peak shifted in voltage depending on either the electrode separation or thin film resistance (see table 1). These

results indicate that the I-V shape and location of current maximum are related to the current density regime which in turn is determined by MNs distribution. The SEM analysis showed that the MNs nanostructure changes after application of an external electric field and this has been attributed to an electroforming process. Metal migration irreversibly changes the morphology and electrical properties of the MN thin film.

Differences in I-V curves and electroformed film morphology which were observed confirm that sorbed species on the surface of the metal thin films and their ability to bridge gaps between metal nanoparticles alter the electroforming process and shifts the critical voltage of breakdown upwards.

It was found that major metal migration processes occurring under vacuum in Pt nanoisland thin films can be prevented at surface coverage levels of about 55% where formed metal percolated layers still show an island structure.

Overall, these results show that for a device containing nanometallic structures there will have to be some form of conditioning process. The nature of this pre-treatment is likely to be dependent on factors such as the type of substrate, metal, the surface coverage of the MN layer and also the atmosphere surrounding the device.

References

[1] Tanner R.E., Goldfarb I., Castell M.R. and Briggs G.A.D, Surf. Sci. 486 (2001), 167-184.

[2] Mandal S.K., Roy R.K. and Pal A.K., J. Phys. D: Appl. Phys. 36 (2003) 261-265.

[3] Choi W.B., Chung D.S., Kang J.H., Kim H.Y., Jin Y.W., Han I.T., Lee Y.H., Jung J.E., Lee N.S., Park G.S. and Kim J.M., Appl. Phys. Lett. 75 (1999) 3129-3131.

[4] Grabowska J., Tobin G., Nanda K.K., McGlynn E., Mosnier J.-P. and Henry M.O., MFMN 2004, Proceedings of Materials for Microelectronics and Nanoengineering, Southampton, U.K., September 13-14, 2004, p.26.

[5] Chengfeng Q., Haiying C., Zhiliang X., Man W. and Hoi-Sing K., SID 2002, Proceedings of The Society for Information Display, Boston, MA, May 19-24, 2002, p.1262.

[6] Arzt E., Kraft O. and Mockl U.E., Materials Reliability in Microelectronics IV. Symposium, San Francisco, CA, USA, April 5-8, 1994, p. 397.

[7] Lee S.H. and Kwon D., Thin Solid Films 341 (1999) 136-139.

[8] Ichinokawa T., Haginoya C., Inoue D., Itoh H. and Kirschner J., Jpn. J. Appl. Phys. 32 (1993) 1379-1384.

[9] Fedorovich R.D., Naumovets A.G. and Tomchuk P.M., Phys. Rep. 328 (2000) 73-179.

[10] Pagnia H. and Sotnik N., Phys. Stat. Sol. A 108 (1988) 11-65.

[11] Neugebauer C.A., in: Maissel L. I. and Glang R. (Eds.), Handbook of thin film technology, McGRAW HILL, New-York NY, 1970, chapter 8.

[12] Bieganski P., Dobierzewska-Mozrzymas E., Newelski M., Pieciul E., Vacuum, 46 (1995) 513-516.

[13] Dearnaley G., Morgan D.V. and Stoneham A.M., J Non-Crystal. Sol. 4 (1970) 593-612.

[14] Blessing R., Pagnia H. and Sotnik N., Thin Sol. Films 85 (1981) 119-128.

Figure and table captions

Figure 1 - SEM images of Pt semi-continuous thin films deposited by DC magnetron sputtering on glass (a) and silicon (b) substrates at 30W for 10 s. The contrast achieved on silicon allowed accurate measurements of the gap between islands. This resulted always very small and less than 3nm in all the cases.

Figure 2 – I-V curves obtained at RT under HV and in air by applying slow velocity (~0.1V/s) DC voltage sweeps up to a limit of 10V across different areas on a glass sample (S1). Both vacuum and air curves present an initial ohmic behaviour followed by a slow decrease in conductance until reaching a current maximum. The current peak shifts with the electrode distance.

Figure 3 – SEM images of electroformed Pt nanoislands thin films on glass. After two voltage sweeps up to 10V (a) under HV and (b) in air (see figure 4) the film microstructure showed in both cases marked morphological changes. In particular, it can be observed that these current-induced effects tend to form and destroy filaments in vacuum while they lead to a filament network in air.

Figure 4 – Current profiles obtained at RT under HV and in air over 1mm areas. While the sample under vacuum exhibits an irreversible change in resistance, the sample in air shows a certain degree of ‘regeneration’.

Figure 5 – SEM/EDX analysis of Pt MN thin film on soda lime glass after I-Vs conducted in vacuum and air. A stronger peak at 0.29keV which can be related to the carbon k-line appears in air samples by comparison with vacuum samples. Other chemical elements included in the spectra relates to typical composition of soda lime glass.

Figure 6 – (a) Spanning clusters configuration and (b) current distribution obtained by simulating the metal percolated layer as a 2D mesh of cells either empty or metallic. Current distribution corresponding to occupation probabilities above 60% typically presented 'hot-spots' (i.e., black cells) along conductive filamentary paths where the current reaches maximum values. These hot-spots could burn out during a voltage sweep, permanently affecting the conductivity of current channels.

Figure 7 – SEM images of MNs films sputtered on glass. Picture (a) refers to the sample S2-0.5mm-HV, while (b) depicts nanoislands distribution corresponding to the sample S3-0.5mm-HV. These pictures show MN distributions corresponding to *LRs* of 10^5 and $10^6\Omega$/m respectively. As the metal film is very thin and less conductive, both images are affected by charging effects which lead to the appearance of 'bright' spots.

Figure 8 – SEM images of MN films on glass after electrical characterisation at RT in HV (see figure 9). Pictures (a) and (b) correspond to 0.5mm areas on samples S2 and S3 respectively. As can be observed by comparison with figures 7a and b, the electroforming has slightly affected the thin film morphology but the MN shape and separation can still be appreciated.

Figure 9 – I-V curves obtained under vacuum at RT for high *LR* 0.5 mm areas (table 1, samples S2 and S3). Along voltage ramps up to 10V, both samples showed an initial ohmic behaviour followed by a non-linear deviation with an increase in sample conductance. Samples S2 shows a higher current density and breaks down at about 10V.

Table 1 – Initial resistance R_0, *LR* values and critical voltages for a set of samples characterised at RT in HV and air.

Pt MN on glass: sample	S1					S2		S3
electrode separation (mm)	0.5	1	1	1.5	2	0.5	0.5	0.5
HV or air	HV	HV	air	air	air	HV	air	HV
R_0 (Ω)	18	27	14	46	72	50	72	456
LR (x 10^4 Ω/m)	3.6	2.7	--	--	--	10^5	--	~ 10^6
V_C (V) – 1st up ramp	6.5	8.8	7.7	13.5	14.5	10.2	16.5	--

Table 1

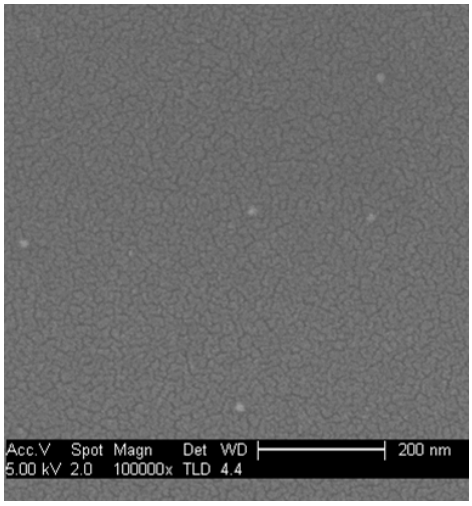

Fig 1a

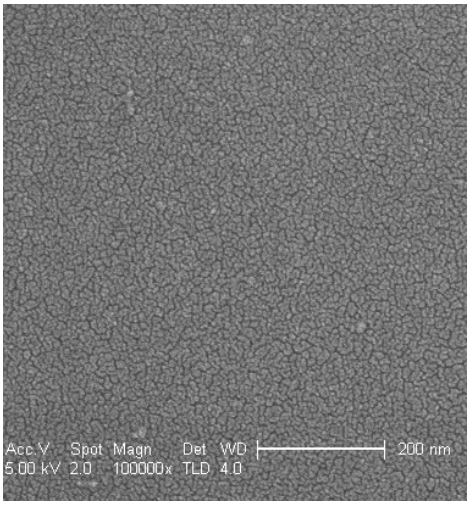

Fig 1b

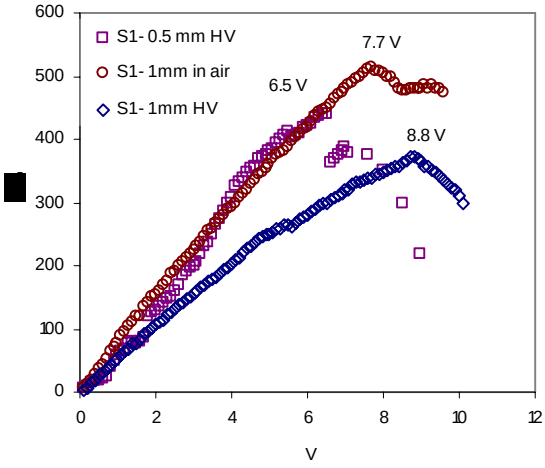

Fig. 2

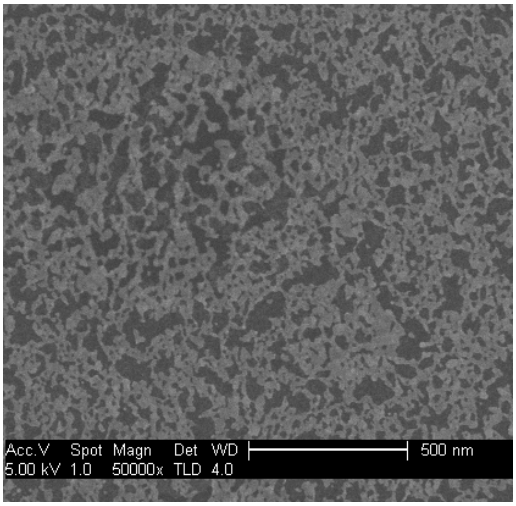

Fig 3a

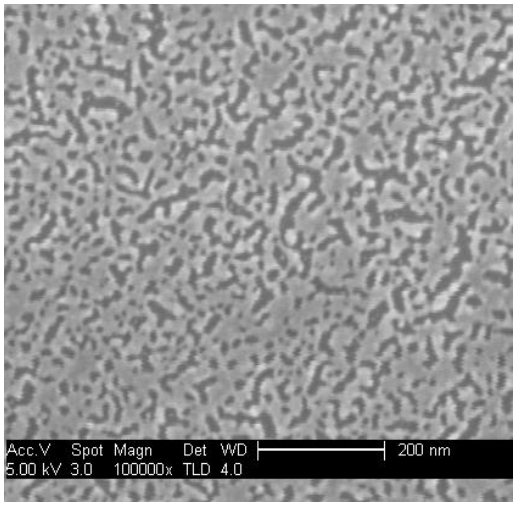

Fig 3b

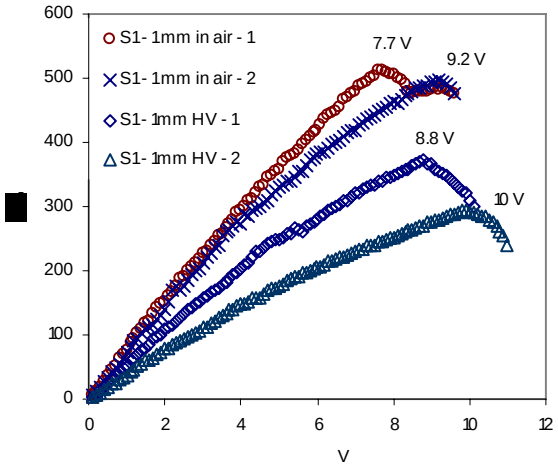

Fig 4

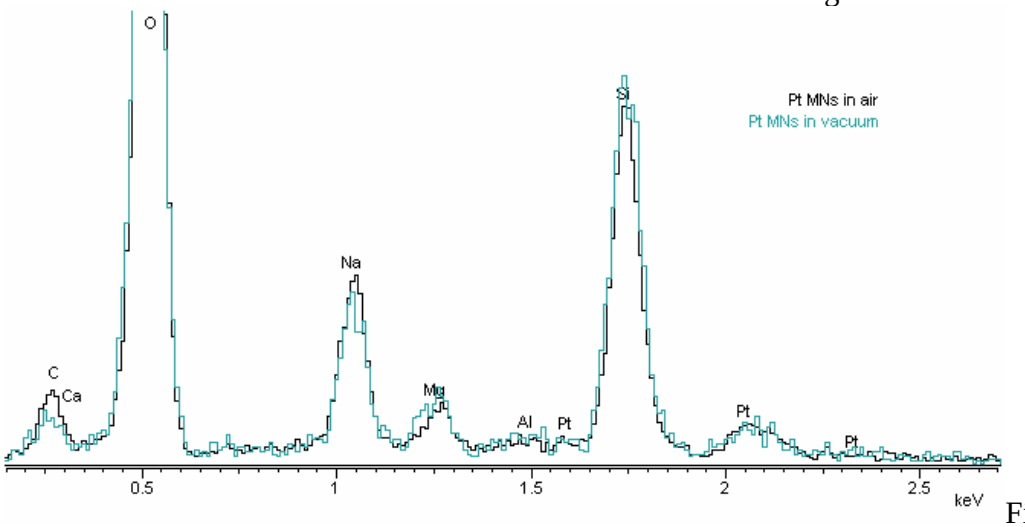

Fig 5

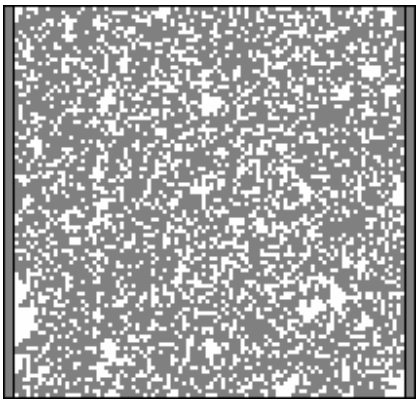

Fig 6a

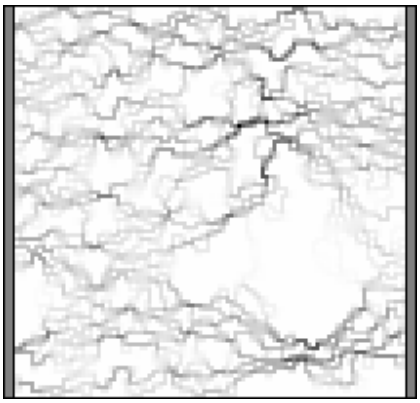

Fig 6b

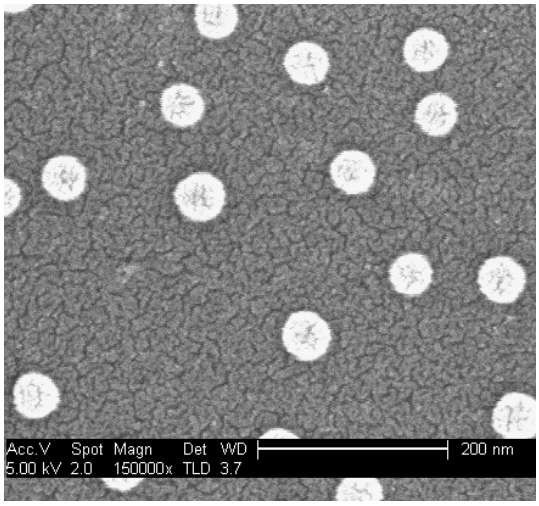

Fig 7a

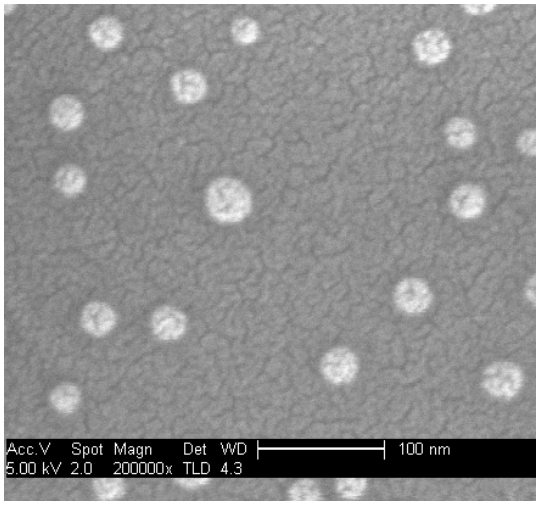

Fig 7b

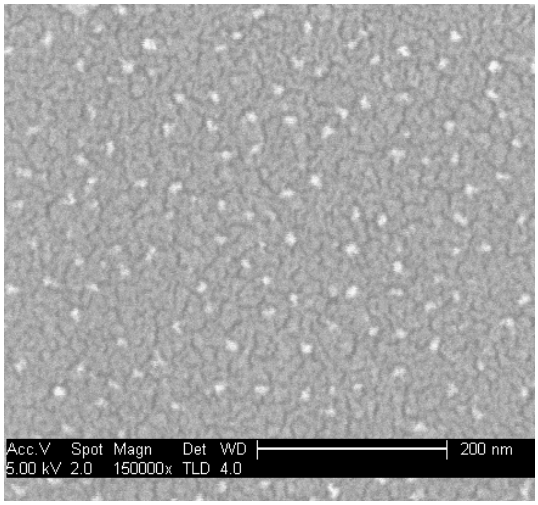

Fig 8a

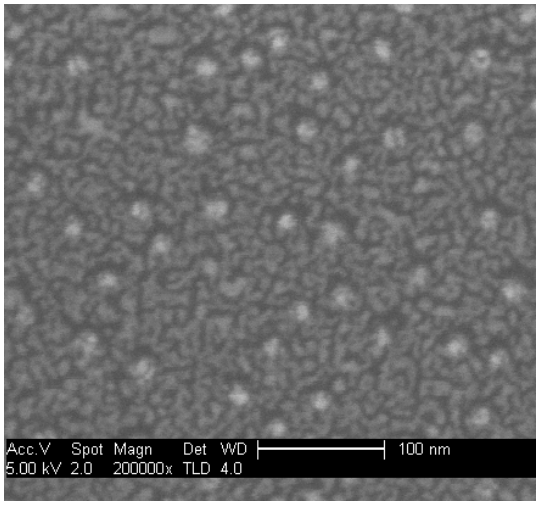

Fig 8b

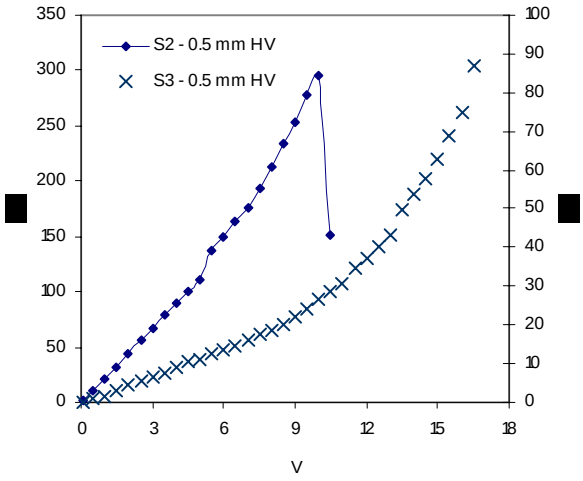

Fig 9